Applied Catalysis A: General 388 (2010) 86–95

Contents lists available at ScienceDirect

Applied Catalysis A: General

journal homepage: www.elsevier.com/locate/apcata

Composition of tungsten oxide bronzes active for hydrodeoxygenation

Timothy J. Thibodeau[a,b,c], Alexander S. Canney[b,c], William J. DeSisto[b,c,d], M. Clayton Wheeler[c,d], François G. Amar[a], Brian G. Frederick[a,b,c,*]

[a] Department of Chemistry, University of Maine, Orono, ME 04469, USA
[b] Laboratory for Surface Science and Technology, University of Maine, Orono, ME 04469, USA
[c] Forest Bioproducts Research Institute, University of Maine, Orono, ME 04469, USA
[d] Department of Chemical and Biological Engineering, University of Maine, Orono, ME 04469, USA

ARTICLE INFO

Article history:
Received 19 November 2009
Received in revised form 13 August 2010
Accepted 17 August 2010
Available online 22 August 2010

Keywords:
Acrolein
Allyl alcohol
Tungsten trioxide
Bronze
Catalyst
Spill-over
Hydrogenation
Hydrodeoxygenation
Thermogravimetric analysis

ABSTRACT

We explore the composition of reduced tungsten oxide bronze materials as a new class of heterogeneous catalysts for hydrodeoxygenation of bio-fuels. We demonstrate a method using thermogravimetric analysis (TGA) and mass spectrometry to determine both the oxygen substoichiometry and hydrogen content of the H_yWO_{3-z} catalytic phase that is formed during hydrogen pretreatment at temperatures from 200 to 500 °C. Results for three WO_3 materials show that the composition depends on crystallinity and surface area, as well as pretreatment temperature and time. The optimal pretreatment conditions for hydrogenation of acrolein to allyl alcohol at 50 °C occur over a narrow temperature range around 350 °C. We report for the first time that at higher reaction temperatures the catalysts are active for hydrodeoxygenation of allyl alcohol to propene and 1,5-hexadiene. We have proposed a mechanism similar to the Mars–van Krevelen cycle in which an alcohol adsorbs on an oxygen vacancy, forming a tungsten–oxygen bond and breaking the carbon–oxygen bond. Our TGA and reaction kinetics data indicate that the composition of the active catalyst is between $H_{0.9}WO_{2.9}$ and $H_{1.3}WO_{2.7}$ and that the rate of hydrodeoxygenation is comparable to the oxygen vacancy creation rate.

1. Introduction

Production of fuels from lignocellulosic biomass has the potential to reduce dependence on fossil fuels and emission of greenhouse gases. Utilization of biomass is important because it is currently the only renewable source of liquid transportation fuels [1,2]. Pyrolysis of biomass is economically feasible at a smaller scale and offers potential energy efficiency advantages over Fischer–Tropsch and fermentation processes. However, pyrolysis produces a complex mixture of oxygenated organic compounds with low energy density due to high oxygen composition and upgrading is necessary [1–3]. Pyrolysis oil is composed of carboxylic acids, aldehydes, ketones, carbohydrates, alcohols and phenols [4–6]. Early work demonstrated that several classes of materials, including supported precious metals and cobalt/molybdenum sulfides, are capable of catalytically removing oxygen from the oil, increasing its energy content and stability [7,8]. Many of the compounds in pyrolysis oil are unsaturated. For economic reasons, we have focused on developing catalysts that can selectively reduce or break carbon–oxygen bonds while minimizing hydrogenation of carbon–carbon double bonds.

As an example of hydrotreating reactions for an unsaturated aldehyde, Fig. 1 illustrates the range of activity and selectivity that has been reported for hydrogenation of acrolein, CH_2=CH-CHO, over a variety of catalysts [9–17]. Most noble metal catalysts have good activity but are very selective to formation of the undesirable product, propanal. Two reducible metal oxide catalysts, as reported by Hoang-Van and Zegaoui [13] facilitate hydrogenation of the carbonyl group, albeit with much lower activity. Molybdenum oxide is selective towards 1-propanol, but both the carbon–carbon double bond and the carbonyl group are hydrogenated. Interestingly, over a reduced tungsten oxide catalyst, only the carbonyl group is hydrogenated, selectively producing allyl alcohol. Hoang-Van and Zegaoui [13] reported that pretreatment in hydrogen at temperatures of 150–350 °C is necessary to achieve activity for both pure MoO_3 and WO_3 catalysts, as well as for Pt/MoO_3 and Pt/WO_3 catalysts, and suggest that the active phase is a hydrogen bronze, H_xWO_3 (where x is non-stoichiometric) [18]. Further evidence that bronzes are active for hydrodeoxygenation of alcohols has been reported: Matsuda et al. have shown that 2-propanol can

* Corresponding author at: Laboratory for Surface Science and Technology, University of Maine, Orono, ME 04469, USA. Tel.: +1 207 581 2268; fax: +1 207 581 2255.
E-mail address: brian.frederick@umit.maine.edu (B.G. Frederick).

0926-860X/$ – see front matter © 2010 Elsevier B.V. All rights reserved.
doi:10.1016/j.apcata.2010.08.025

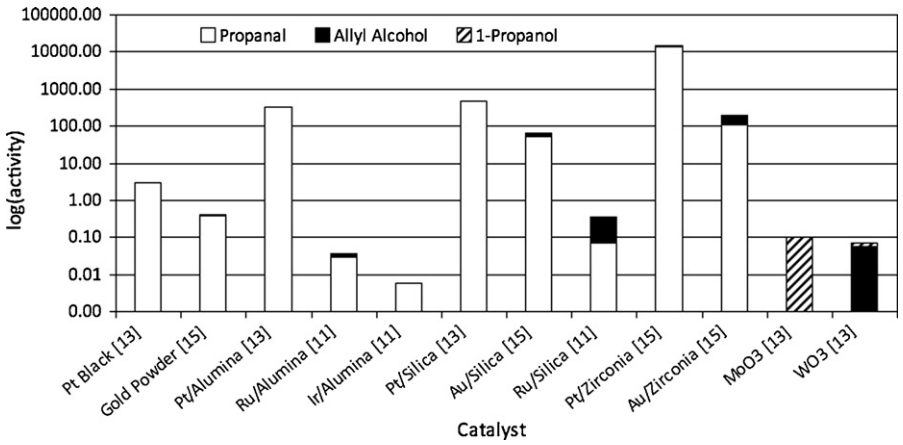

Fig. 1. Comparison of the activity (on a log scale) for hydrogenation of acrolein over a selection of catalysts (references identified in brackets). Selectivity toward propanal, 1-propanol, and allyl alcohol is indicated as the fraction of each product (on a linear scale) [11,13,15].

be converted to propene over a molybdenum oxide bronze [19] and Herrera et al. have shown that WO_3/SBA-15 is active for the dehydration of methanol and 2-butanol [20].

Reducible metal oxide catalysts, such as bismuth molybdate, vanadia, and tungsten oxide, have long been known as selective oxidation catalysts [21]. The widely accepted Mars–van Krevelen mechanism [22] involves selective oxidation of olefins to aldehydes, where the oxygen in the product comes directly from the oxide lattice. In a parallel theoretical study, we have explored the factors controlling hydrodeoxygenation of acrolein to produce propene, 1-propanol, and allyl alchohol on reduced MoO_3 surfaces [23]. The mechanism for propene production, shown schematically in Fig. 2, involves hydrogen adsorption, formation of oxygen vacancies via water production, selective adsorption of acrolein at the vacancy, hydrogenation of the carbonyl to an allyl alkoxide intermediate, and C–O bond scission leading to propene. Thus, we proposed that the active state of the catalyst is a reduced metal oxide bronze. Both Hoang-Van and Zegaoui [18] and Matsuda et al. [19] suggest, based on XRD, that the catalyst is a bronze, but do not quantify the hydrogen content or consider oxygen substoichiometry.

Although thermogravimetric methods have been used to characterize tungsten oxide bronzes formed through solid state and electrochemical reactions [24], we are not aware of materials characterization work that determines simultaneously the composition of hydrogen and oxygen when the bronze is formed under prolonged hydrogen treatment of tungsten oxide at atmospheric pressure in the 300–500 °C range. There is general agreement that loss of oxygen does not occur at temperatures below 200 °C [25]. Under typical temperature ramp conditions, 5 °C/min in flowing H_2, reduction of WO_3 is not observed until 600 °C [25]. Lackner et al. [25] have studied the reduction of commercial tungsten oxide at temperatures between 800 and 1000 °C under isothermal conditions. They report that in this high temperature range the oxide is reduced to tungsten metal, as determined by a weight loss of 20.7%.

Previous studies using thermogravimetric analysis have also investigated hydrogen reduction with noble metals dispersed on WO_3 [26–29]. In most high temperature ramp thermogravimetric analysis (TGA) experiments, the addition of metals causes weight loss, corresponding to oxygen substoichiometry, to occur at lower temperatures than on the pure WO_3. Only in a study by Kanamaru et al. [27] were low temperature isothermal TGA experiments performed. They prepared 0.1 and 0.01 wt% Pt/WO_3 by impregnation with H_2PtCl_6, converting the WO_3 to H_xWO_3. The catalysts were calcined in air and cooled in argon. Then, the WO_3 was treated in 10% H_2/Ar at temperatures of 40–200 °C. At these temperatures, they report a weight *gain* due to the addition of hydrogen to the bronze. The maximum weight gain measured is 0.098%, which corresponds to the composition of $H_{0.3}WO_3$, assuming no oxygen loss.

In this paper, we first describe a method using TGA and mass spectrometry to determine the composition of a reduced metal oxide bronze. We report the composition of bronzes made from three different tungsten oxide materials at temperatures of 300–500 °C. We then show that the activity for acrolein hydrogenation to allyl alcohol occurs over a narrow pretreatment temperature range and is critically dependent on the amount of hydrogen in the bronze. Next, we report the activity and selectivity of bronzes, pretreated at 350 °C, for hydrogenation and hydrodeoxygenation of allyl alcohol. At 50 °C, propanal is the major product, with lesser amounts of 1-propanol, differing somewhat from the results of Hoang-Van and Zegaoui [13]. At higher temperatures, we observe good hydrodeoxygenation activity, mostly to propene and 1,5-hexadiene. We analyze the product distribution to place limits on the composition of the active phase and suggest that selectivity toward hydrodeoxygenation is limited kinetically by the C–O bond activation barrier, while hydrogenation is facile and the products are largely controlled by thermodynamics.

2. Experimental

2.1. Materials

Three types of non-porous tungsten oxide were examined, a commercially available material of 30–70 nm particle size (Sigma–Aldrich Tungsten(VI) oxide, nanopowder, <100 nm (TEM)) that we refer to hereafter as "nano-WO_3"; a material prepared at UMaine by Lu and Tripp [30] by emulsion polymerization that we refer to as "UM-WO_3"; and a commercially available material of 20 μm particle size (Sigma–Aldrich) that we refer to as "20 μm-WO_3."

Nitrogen adsorption isotherms were measured at 77 K using a Micromeritics ASAP-2020 instrument. The WO_3 was degassed for 4 h at 150 °C. The adsorption isotherms and corresponding pore size distributions, as calculated with the BJH method [31,32], showed no evidence of pores. Surface areas were calculated using the BET method [33]. The nano-WO_3 had a surface area of 9.1 m^2/g, UM-WO_3 had a surface area of 3.0 m^2/g, and 20 μm-WO_3 had a surface area of 1.5 m^2/g.

Powder X-ray diffraction measurements were made on all three materials using a PANalytical X'PertPro X-Ray diffractometer utilizing Cu-Kα radiation in a parallel beam optical configuration. The diffraction patterns, shown in Fig. 3, were very similar to those reported previously by Lu et al. [30]. The crystalline phase was

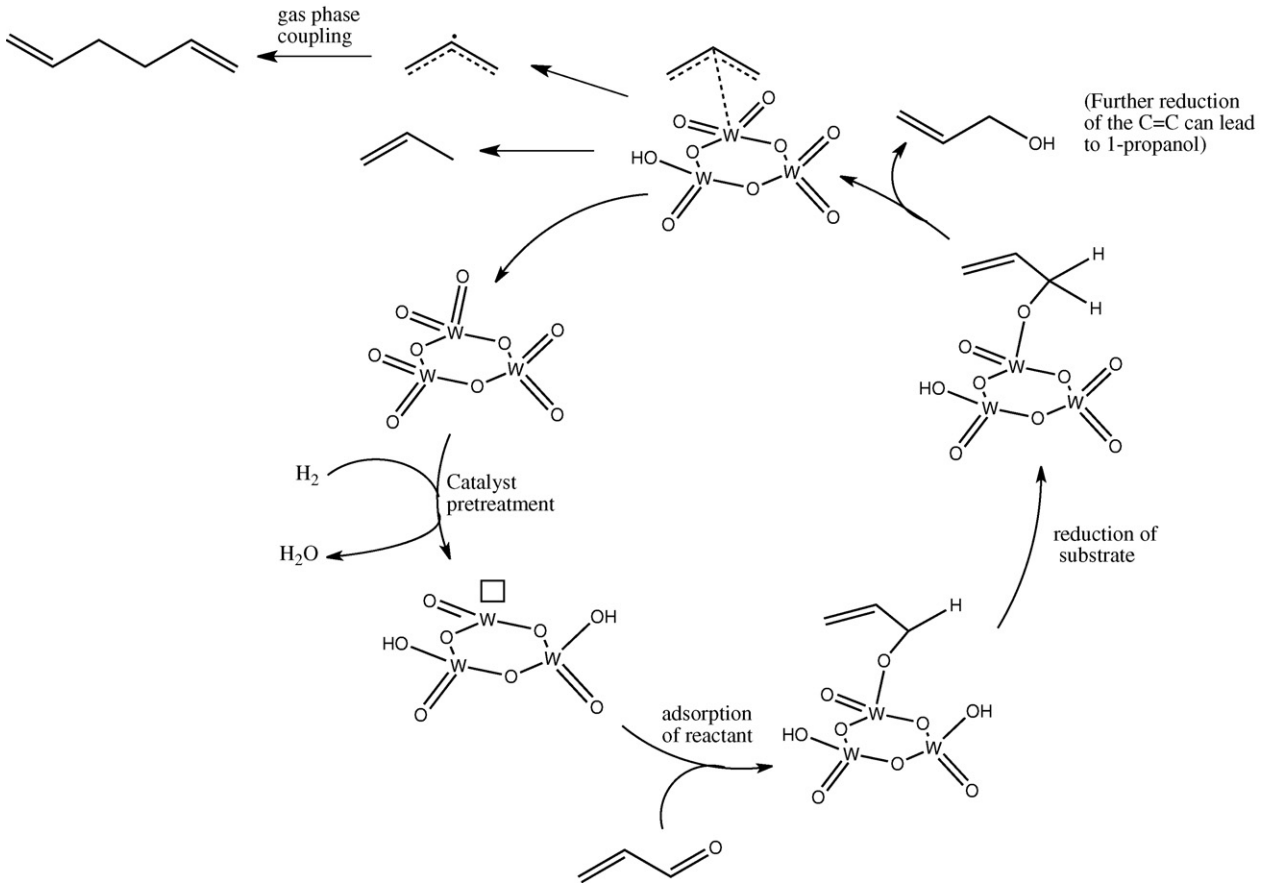

Fig. 2. Schematic mechanism proposed for the hydrodeoxygenation activity of reduced metal oxide bronzes.

ascribed to monoclinic WO_3. However, the broad background, centered at $2\theta = 16–17^\circ$, indicates significant amounts of amorphous material, which is greatest in the UM-WO_3.

2.2. Catalyst activation and bronze composition

The WO_3 catalysts were pretreated and tested in a fixed bed reactor, described previously [34]. An amount of WO_3, corresponding to 0.75 m^2 surface area, was supported on 0.5 g of crushed quartz (90–180 μm particle size) which was packed into a 0.25 in. OD stainless steel glass lined reactor tube (AMI). A thermocouple inside a thermal well allowed the internal bed temperature to be measured directly and was used for temperature control during hydrogen pretreatment and reaction measurements. We note that

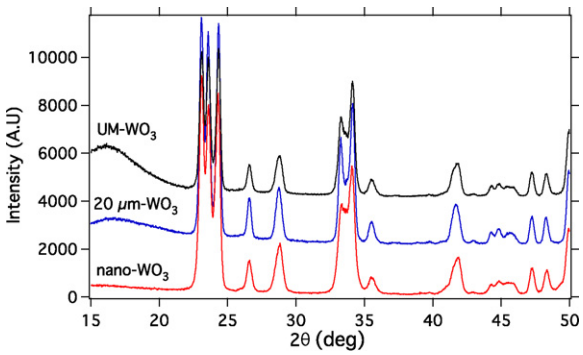

Fig. 3. X-ray diffraction patterns of three tungsten oxide materials (as prepared/supplied). Patterns for 20 μm-WO_3 and UM-WO_3 displaced vertically by 2000 and 4000, respectively, for clarity.

internal bed temperatures during the highly exothermic pretreatment reaction could be as much as 200 °C higher than the external temperature. The catalyst was pretreated in pure hydrogen (Parker Ballston PEM-500, >99.999%) for periods of 3–10 h at temperatures between 200 and 450 °C. In the TGA oven, the bronzes were prepared, starting from fresh samples of WO_3, under the same conditions used in the reactor. The oxide was heated to the specified temperature and held for 10 h in pure hydrogen at atmospheric pressure, flow 90 sccm, then cooled to 50 °C.

Bronze composition was quantified in the TGA from the weight changes during two reaction steps for each formation temperature. The mass loss during bronze formation is the difference between oxygen weight loss and hydrogen weight gain. To determine both the hydrogen content and the oxygen substoichiometry, in Step 1, the bronze was purged with nitrogen, then heated to 1000 °C at a ramp rate of 20 °C/min. The mass lost due to reaction of hydrogen in the bronze with lattice oxygen produced water, which was confirmed with mass spectrometry. The sample was then cooled to 50 °C and purged with oxygen. In step 2, the reduced oxide was heated in oxygen to 1000 °C at a ramp rate of 20 °C/min to reoxidize the catalyst to WO_3, allowing us to determine the total of the oxygen substoichiometry in the bronze and the additional amount of oxygen lost in Step 1. We elaborate on the physical evidence supporting the proposed method and numerical procedures utilized in determining the composition of the bronze, H_yWO_{3-z}, in Section 4.

The evolved gases were monitored via a 50 μm ID quartz capillary sampling system (AMETEK) using a mass spectrometer (Stanford Research Systems, RGA 300) housed in a turbo-molecular pumped vacuum chamber. Approximately 100 mg of WO_3 powder was placed on either an alumina or platinum pan in the TGA oven. Blank experiments, with both ceramic and platinum pans (with-

out WO_3), showed that uptake of hydrogen was negligible. A gas handling manifold allowed switching between hydrogen (grade 5.0, Matheson Tri-Gas) or oxygen (grade 5.0, BOC Gas) after flushing the TGA system with house nitrogen (blow-off from a liquid nitrogen dewar) for safety reasons. Control experiments confirmed that, without hydrogen pretreatment of WO_3, cycles of heating to 1000 °C in nitrogen and oxygen resulted in weight changes of 0.1% or less.

2.3. Reaction characterization

After pretreatment, the catalyst was cooled to room temperature in hydrogen. Then the reactor was heated to reaction temperature (between 50 and 350 °C). Reactant vapor was supplied by a vapor liquid equilibrator (VLE) at 10–12 °C using nitrogen carrier gas (BOC, grade 5.0) and blended with hydrogen (Parker Ballston PEM-500, >99.999%) controlled by separate mass flow controllers. The flow rates of nitrogen carrier and hydrogen were both 10 sccm (cm^3/min at 0 °C and 1 atm). The estimated vapor pressures of acrolein (Alfa Aesar, 97%, stabilized) and allyl alcohol (Acros, >99%) were 88 and 4 torr, respectively. Typical total flow rates were 20 sccm corresponding to space velocities of 1800–3400 h^{-1}. Mass hourly space velocities for acrolein were 2.0–2.4 g/h g WO_3 and for allyl alcohol were 1.6–11.7 g/h g-WO_3 for the temperatures and pressures studied.

The product distribution was analyzed using GC-MS (Thermo Trace) for compound identification and GC-FID (Thermo Trace) for quantification. Switching valves allowed sampling upstream and downstream of the reactor bed to estimate conversion. The injector and FID were heated to 250 °C. The column flow rate was 1.5 mL/min and the split ratio was 50. A stabilwax column (Restek, 30 m, 0.32 mm, 20 μm) was used to separate acrolein, allyl alcohol, 1-propanol and 1,5-hexadiene. The GC program consisted of a 5 min hold at 40 °C, a ramp to 150 °C at 10 °C/min followed by a 2 min hold. We used a PLOT Q column (HP, 30 m, 0.32 mm, 20 μm) to separate ethene, ethane, propene, propane, and 1,5-hexadiene; however, allyl alcohol was poorly separated from 1-propanol. The GC program consisted of an initial hold at 80 °C for 1 min, a ramp to 250 °C at 20 °C/min, and a 5 min hold. To measure light gases (CO, CO_2), a J&W Gas Pro column was used (60 m, 0.32 mm) with MS detection. To separate CO, CO_2, and nitrogen the column was cooled to −80 °C with liquid nitrogen and held for 3 min. Then, the GC oven was heated to 250 °C at 25 °C/min and held for 5 min.

To close the mass balance on allyl alcohol, FID sensitivity factors were estimated based on the number of carbons less the number of oxygens. At low reaction temperatures, adsorption of allyl alcohol on the catalyst surface accounted for a majority of the apparent conversion, which was confirmed by an isothermal desorption experiment. Initially, the catalyst was exposed to allyl alcohol for a period of 4 h at 50 °C. The allyl alcohol was switched out and the downstream mixture was sampled every 15 min for 2 h by GC-FID with only hydrogen flowing over the catalyst. The allyl alcohol evolved accounted for 95% of the apparent conversion. A subsequent temperature programmed reaction measurement, at a ramp rate of 5 °C/min to 350 °C, produced additional allyl alcohol and other reaction products.

3. Results

3.1. Composition of reduced bronze catalysts (H_yWO_{3-z})

Fig. 4 illustrates the mass changes, temperature program, and mass spectrometer signals during bronze formation and the two analysis steps used to determine the composition of the reduced tungsten bronze. While flowing hydrogen over the oxides at elevated temperatures, a mass loss is measured which is mostly due to loss of oxygen as water, as indicated by the mass spec signal. Fig. 4A shows that at lower temperatures (300–350 °C) the mass loss is small and approaches steady state. The composition of the bronze formed during pretreatment in this temperature range can be controlled precisely. As the temperature is increased above 350 °C the rate of mass loss is much faster, so controlling the composition is more difficult. By 450 °C the mass loss is 20%, which corresponds to complete reduction to tungsten metal.

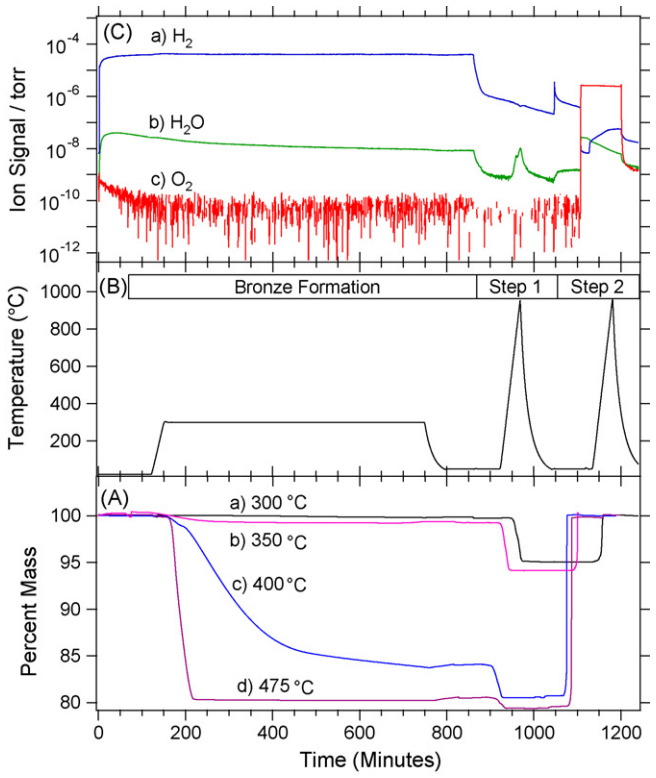

Fig. 4. Illustration of the TGA and MS data during bronze formation, and a two-step method to determine composition. (A) Percent weight change on a ceramic pan loaded with the nano-WO_3 (9 m^2/g) at (a) 300 °C, (b) 350 °C, (c) 400 °C, and (d) 475 °C bronze formation temperatures. Illustration of (B) temperature profile and (C) mass spectral intensities for a) hydrogen (2 amu), (b) water (18 amu), and (c) oxygen (32 amu) vs. time for 350 °C bronze formation temperature.

To determine the hydrogen content, the catalyst was heated in nitrogen (Step 1). The hydrogen reacts with lattice oxygen, producing the water desorption peak shown in Fig. 4C(b). In Step 2, after switching to oxygen and heating, the reduced oxide (WO_{3-x}) formed at the end of Step 1 gains weight to within 0.1% of its initial value, corresponding to WO_3. The weight gain corresponds to recovery of the oxygen lost during bronze formation and the lattice oxygen lost to water formation in Step 1.

Fig. 5 shows the mass change for (A) bronze formation, (B) Step 1, and (C) Step 2 for the three materials on a ceramic pan. In general, as the temperature is increased during the bronze formation step, the mass loss increases. Over the 300–400 °C range, the mass loss also correlates with surface area, suggesting that the oxygen substoichiometry depends on surface area. However, the weight change in Step 1 at temperatures below 350 °C was similar for all three materials, indicating a similar hydrogen content. At temperatures of 300–350 °C the mass loss (due to H_2O desorption) in Step 1 was similar to the mass gain (due to oxygen) in Step 2. Because these mass changes were much larger than the mass loss during bronze formation, the hydrogen stoichiometry, y, should be large compared to the oxygen substoichiometry, z, i.e. the bronzes formed at these temperatures were close to H_yWO_{3-z}, with $y \gg z$. At higher

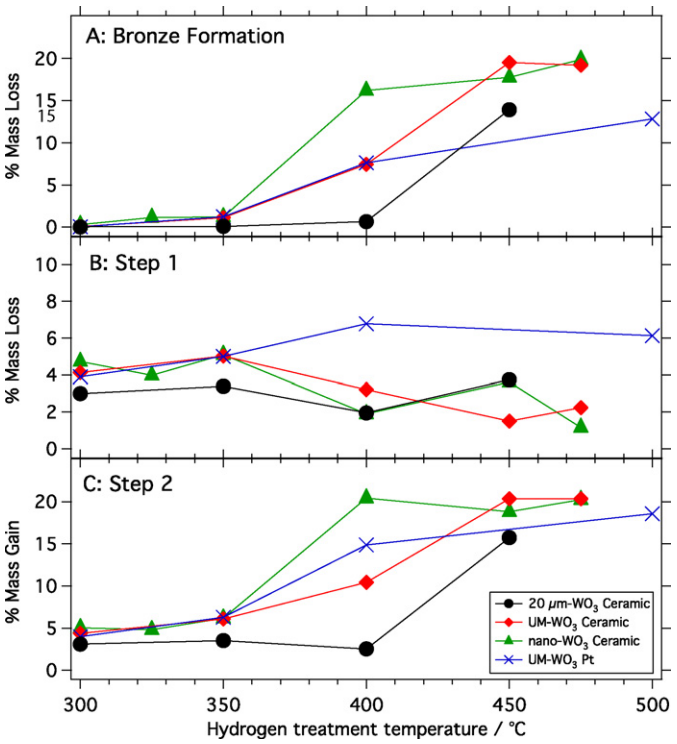

Fig. 5. Weight loss or gain during (A) bronze formation in hydrogen, (B) heating in nitrogen (Step 1), and (C) heating in oxygen (Step 2) as a function of the hydrogen treatment temperature for the 20 μm-WO_3, UM-WO_3 and nano-WO_3 materials using ceramic or platinum TGA pans, as indicated.

temperatures, the weight gain in Step 2 is larger than the mass loss in Step 1, and similar to the mass loss during bronze formation, which suggests that the bronze has a composition H_yWO_{3-z}, with $y < z$. These qualitative trends in the bronze composition are confirmed quantitatively by our analysis given in Section 4.

Because noble metals are used as spillover catalysts in hydrogen storage materials, we also compared the data for the UM-WO_3 to experiments on a platinum pan. In Step 1, there is a larger mass loss above 350 °C on platinum compared to the ceramic pan, which corresponds to a higher hydrogen content. This shows that significant hydrogen uptake occurs over macroscopic distances. At temperatures up to 400 °C, the mass changes during bronze formation are similar. Above 400 °C, when the ceramic pan is used the oxide is reduced completely to metal while on a platinum pan it is not as heavily reduced, suggesting that hydrogen increases the stability of the tungsten oxide lattice.

3.2. Hydrogenation of acrolein to allyl alcohol

Hoang-Van and Zegaoui have shown that the hydrogenation of acrolein requires that the catalyst be pre-treated in hydrogen and that the activity is sensitive to the pretreatment conditions [13]. We have measured the acrolein hydrogenation activity as a function of pretreatment temperature under similar, 3 h conditions using the UM-WO_3 material. The activities are summarized in Fig. 6, and compared to those of Hoang-Van and Zegaoui [13]. The activity is probably lower for our catalysts because of lower surface area and lower partial pressure of acrolein. The peak in activity in our results occurs 200 °C higher than theirs, which may be due to surface area dependence or could be attributed to inaccuracies in bed temperature measurement, as noted in the Experimental section. The hydrogenation activity occurs over a narrower pretreatment temperature range in our results.

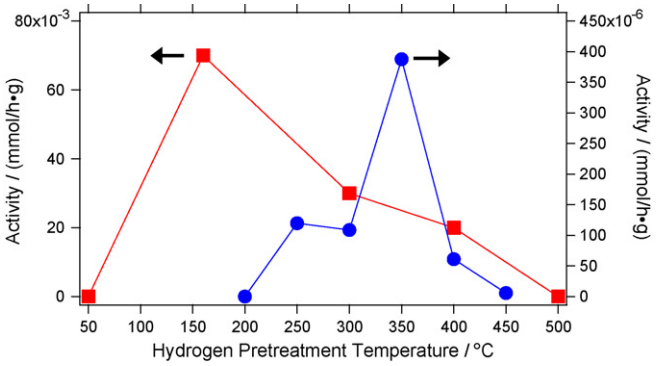

Fig. 6. Dependence of acrolein hydrogenation activity at 50 °C after pretreatment in hydrogen for 3 h at the indicated temperature for UM-WO_3 (circles) compared to results of Hoang-Van and Zegaoui [13] (squares).

Interestingly, if the tungsten oxide is reduced at 250 °C for 3 h we notice that in the succeeding reaction, the catalyst is selective towards the formation of 1-propanol for 2 h, then allyl alcohol is produced at a much lower rate for an additional hour before the catalyst loses activity. This shows that initially, there is enough hydrogen in the catalyst to completely hydrogenate acrolein to 1-propanol but the rate of hydrogenation is faster than the rate of hydrogen dissociation so the selectivity shifts from 1-propanol to allyl alcohol. The amount of hydrogen consumed in the production of allyl alcohol and 1-propanol agrees with the amount of hydrogen in the bronze, based on the TGA experiments, to within experimental errors.

By extending the pretreatment duration from 3 to 10 h, we found that the catalyst maintained steady state activity for days. This suggests that under reaction conditions, hydrogen in the bronze can be replenished through H_2 dissociation on oxygen vacancyz sites.

We repeated the experiment with the 20 μm-WO_3 and nano-WO_3 samples and neither exhibited substantial activity for the hydrogenation of acrolein. We suggest that the differences in activity may relate to the amount of amorphous phase present in each sample, as shown in X-ray diffraction patterns (Fig. 3). As we will show, the UM-WO_3 bronze has a higher amount of hydrogen as compared to the other materials under the same pretreatment conditions.

3.3. Hydrodeoxygenation (HDO) of allyl alcohol

The reactivity of allyl alcohol was measured on all three materials at four temperatures between 50 and 350 °C after hydrogen pretreatment at 350 °C for 10 h. A summary of the initial selectivity of each catalyst at each reaction temperature is shown in Fig. 7 and Table 1. The product distribution and activity was different on each of these materials, although all the materials are active for isomerization to propanal and hydrogenation to 1-propanol at 50 °C. By comparison, Hoang-Van and Zegaoui [13] report 100% selectivity toward 1-propanol after pretreatment at 300 °C and similar amounts of propanal and 1-propanol after 400 °C pretreatment. We report, for the first time, that hydrodeoxygenation products were formed at higher temperatures (above 150 °C).

As shown in Fig. 7, at lower temperatures, a large proportion of the apparent conversion is attributed to adsorption. After allyl alcohol reaction for 4 h at 50 °C, an isothermal desorption experiment at 50 °C accounted for most of the reactant. A small amount of reaction products desorbed during subsequent temperature programmed desorption. We note that all three catalysts hydrogenated the C=C bond to form 1-propanol, whereas only the UM-WO_3 was

Table 1
Percent conversion and yield of products on basis of allyl alcohol molar flow rate as a function of reaction temperature for each catalyst pretreated for 10 h at 350 °C.

	Catalyst											
	20 μm WO_3				UM-WO_3				nano-WO_3			
Reactor Temperature (°C)	50	150	250	350	50	150	250	350	50	150	250	350
% Conversion	13.00	13.00	38.00	37.00	8.00	15.00	49.00	26.00	7.00	35.00	61.00	40.00
Ethene	0.00	0.01	0.15	0.65	0.00	0.02	0.29	0.14	0.00	0.04	0.28	0.08
Ethane	0.00	0.01	0.08	0.24	0.00	0.01	0.11	0.05	0.00	0.03	0.13	0.03
Propene	0.01	0.18	2.17	5.96	0.00	0.11	1.90	2.93	0.00	0.12	2.67	4.99
Propane	0.00	0.00	0.02	0.07	0.00	0.00	0.02	0.01	0.00	0.00	0.03	0.01
Acrolein	0.03	0.09	0.20	1.73	0.16	0.16	17.59	1.31	0.16	5.84	22.01	2.22
Propanal	0.23	2.76	10.17	8.35	0.16	2.44	17.75	3.56	0.16	6.02	22.25	2.30
1-Propanol	0.13	4.05	7.37	3.12	0.03	3.85	11.16	0.85	0.01	1.00	16.53	0.00
1,5-Hexadiene	0.01	0.02	0.80	5.05	0.04	0.03	0.87	4.13	0.03	0.03	0.19	0.03

able to hydrogenate the C=O bond of acrolein (Section 3.2). This suggests that the sites for hydrogenation of alkenes are different from those for hydrogenation of carbonyls.

As reported in Fig. 7 and Table 1, we see conversion of allyl alcohol back to acrolein at temperatures above 150 °C. This is consistent with thermodynamic control, since acrolein becomes thermodynamically more favorable than allyl alcohol at temperatures above 150 °C. At most temperatures and on most catalysts, the yield of propanal is greater than 1-propanol, despite the fact that only at reaction temperatures above 277 °C is the formation of propanal more favorable than 1-propanol. Thus, the propanal in the product distribution appears to be kinetically controlled.

The formation of hydrodeoxygenation products (primarily propene and 1,5-hexadiene) is observed only at high reaction temperatures, even though the Gibbs free energy of reaction is highly favorable over the entire temperature range due to the co-production of water. This indicates that the activation barrier for C–O scission must be high, limiting the production of HDO products.

In addition to the HDO products, acrolein, and propanal observed at 350 °C, there was small amounts of CO and CO_2. There was little evidence for coking on the basis of carbon-nitrogen analysis. Thus, we were not able to quantitatively close the mass balance at high temperatures.

The time dependence of the selectivity of all three catalysts at 350 °C is shown in Fig. 8. The major hydrodeoxygenation products, propene and 1,5-hexadiene, decay to a steady state value. On the 20 μm-WO_3, propanal and 1-propanol are relatively constant with time, whereas on the other materials they decay. At steady state, the HDO products predominate on the higher surface area materials.

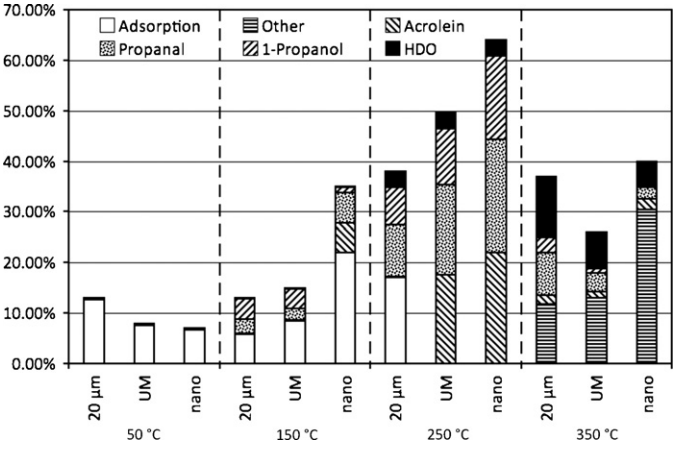

Fig. 7. Comparison of conversion (*y*-axis, total bar height) and selectivity (proportion of bar height) as a function of catalyst and reaction temperature (*x*-axis) for three tungsten oxide bronzes with different surface areas. HDO products formed at higher reaction temperatures include propene, 1,5-hexadiene, propane, ethene, and ethane.

4. Discussion

4.1. Stoichiometry of the bronze

When tungsten oxide is heated in hydrogen, at temperatures below 200 °C, weight increases are observed when platinum facilitates spill-over [25], indicating absorption of hydrogen to form a bronze. Our data for 200 °C, taken on a ceramic pan also shows a weight gain. At temperatures of 300 °C and higher, a net weight loss is always reported [25,26]. The loss of oxygen during hydrogen treatment outweighs the gain due to hydrogen absorption. Theoretical calculations for MoO_3 suggest that the most favorable route to loss of oxygen is through formation of water [35]. Formation of an oxygen vacancy with production of water has a calculated reaction energy of −0.2 eV, while formation of hydroxyls requires 4–4.5 eV

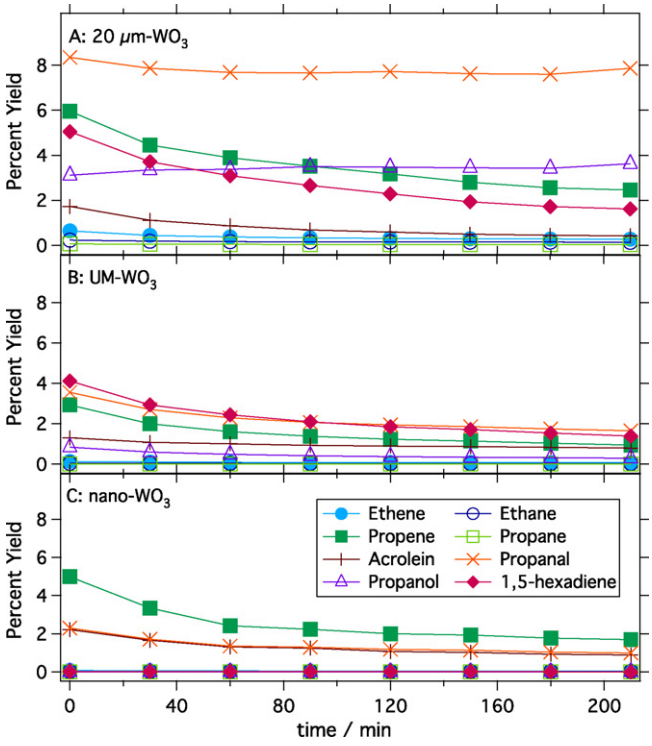

Fig. 8. Time dependence of product distribution on (A) 20 μm-WO_3, (B) UM-WO_3, and (C) nano-WO_3 as a function of time showing that the hydrodeoxygenation rate (propene, 1,5-hexadiene, ethene) decays toward a steady state value but the selectivity of HDO to isomerization products increases with surface area.

and desorption of atomic oxygen 6.5–6.8 eV, depending on the lattice site [35]. Therefore, we write a chemical reaction for the initial hydrogen reduction step in terms of water production,

$$WO_3 + H_2(g) \rightarrow H_yWO_{3-z} + zH_2O(g). \quad (1)$$

As shown in Fig. 4, water production was confirmed using mass spectrometry. The amount of water produced during the nitrogen step was calculated from the mass loss in TGA, which is directly related to the amount of hydrogen dissolved in the bronze. Because the atomic weight of oxygen, A_O, is 16 times that of hydrogen, A_H, an initial estimate of the oxygen substoichiometry coefficient, z, can be calculated from the fractional weight loss during bronze formation in hydrogen, w_H,

$$z_0 = \frac{w_H M_{WO_3}}{A_O}, \quad (2)$$

where M_{WO_3} is the molecular weight of WO_3. Since tungsten oxide is 20% oxygen by weight, w_H cannot be greater than 0.207.

To independently determine the hydrogen content during pretreatment, the bronze was heated in nitrogen to 1000 °C in Step 1. Assuming that the weight loss during the nitrogen step was primarily due to loss of water,

$$H_yWO_{3-z} \rightarrow \tfrac{1}{2}yH_2O(g) + WO_{3-x}, \quad (3)$$

we obtained an initial estimate of the hydrogen stoichiometric coefficient, y_0,

$$y_0 \approx 2\left(\frac{w_N M_{WO_3}}{M_{H_2O}}\right), \quad (4)$$

from the fractional weight loss in Step 1, w_N, where M_{H_2O} is the molecular weight of H_2O. As noted, without hydrogen pretreatment, heating WO_3 in nitrogen to 1000 °C resulted in a weight loss less than 0.1%, illustrating the necessity of dissolved hydrogen in producing significant weight losses.

To determine the oxygen substoichiometry at the end of Step 1, the reduced tungsten oxide was heated in oxygen in Step 2. In all cases, the weight gain restored the WO_3 to within 0.1% of its initial weight. From the stoichiometry of the oxidation reaction,

$$WO_{3-x} + \tfrac{1}{2}xO_2 \rightarrow WO_3, \quad (5)$$

we calculate, the oxygen substoichiometric coefficient, x, from the fractional weight gain in Step 2, w_O

$$x = \frac{w_O \cdot M_{WO_3}}{A_O}. \quad (6)$$

To the extent that hydrogen bronze formation occurred (i.e. $y_0 > 0$), the initial estimate of the substoichiometric coefficient, z_0, is an underestimate, and from the stoichiometry of Reaction (3), we were able to determine y and z iteratively, using

$$z_i = \frac{w_H M_{WO_3} + y_{i-1} A_H}{A_O} \quad (7)$$

$$y_i = 2(x - z_i) \quad (8)$$

which converged to within 0.01% after 4–5 iterations, and the coefficients x, y satisfied

$$w_H = \frac{M_{WO_3} - M(H_yWO_{3-z})}{M_{WO_3}} \quad (9)$$

to within 0.01%. Table 2 summarizes the values of x, y, and z from the weight changes summarized in Fig. 5.

4.2. Factors affecting bronze composition

Quantitative analysis of the oxygen substoichiometry, z, shown in Table 2, for bronze formation in the 300–400 °C range, indeed shows that the substoichiometry correlates strongly with surface area. The hydrogen stoichiometry, y, generally peaks around 350 °C pretreatment temperature, but there is no correlation with surface area. The hydrogen content is highest in the UM-WO_3, which appears to have the largest proportion of amorphous material from the XRD data. However, the correlation between hydrogen content and crystallinity is not clear when comparing the other two materials. For all materials in the ceramic pan, and at temperatures up to the optimal pretreatment temperature of 350 °C, hydrogen was more likely to dissolve and the oxide was not heavily reduced. This is shown by the large value of y (around 1) and the low value of z (less than 1). At higher temperatures the oxide was more heavily reduced and the amount of dissolved hydrogen decreased, yielding values of y less than 1 and z greater than 2.5.

Hydrogen spillover phenomena are widely known for platinum particles dispersed on reducible oxides [27] and are discussed by Hoang-Van and Zegaoui [18] with respect to pretreatment of platinum supported molybdenum and tungsten oxide catalysts. Comparison of reduction of the UM-WO_3 on ceramic vs. platinum pans showed no differences in weight loss during H_2 pretreatment within the uncertainties of the experiment. However, the weight loss in Step 1 between 400 and 500 °C shows significant differences, implying that greater amounts of hydrogen were present in the bronze if a platinum pan was used. By comparison with the same material on the ceramic pan, the value of y for UM-WO_3 is even larger than at 350 °C. At the same high temperatures, the oxygen substoichiometry parameter, z, is not as large on the platinum pan as on the ceramic pan. This suggests that the thermodynamics of the ternary phase are rather complex and that hydrogen stabilizes the lattice oxygen.

The rate of oxide reduction increases with temperature and increasing surface area of the catalysts. The TGA curves for several temperatures are shown in Fig. 4A for the nano-WO_3 on a ceramic pan. At temperatures below 400 °C, the weight change is small and slow. At higher temperatures (475 °C) the oxide reduces completely to metal very quickly. The rate of reduction is generally believed to be controlled by the rate of the surface chemical reaction, rather than diffusion of oxygen vacancies to the surface of the particle [36]. In previous isothermal TGA experiments [25,37,38] in the temperature range from 600 to 1000 °C, an initial parabolic mass loss is observed as the oxide converts from WO_3 to $WO_{2.9}$, followed by three approximately linear regions corresponding to phase changes from $WO_{2.9}$ to $WO_{2.72}$, $WO_{2.72}$ to WO_2, and WO_2 to W. The discontinuities between linear segments in the mass loss curve agree reasonably well with the crystallographic phases $W_{20}O_{58}$, $W_{18}O_{49}$, and WO_2 that are known from diffraction. In these linear segments, the overall rate of mass loss is controlled by the movement of the hydrogen front down through the bed [37] and therefore the rate of mass loss is limited by mass transfer processes, not the chemical reaction rate. The activation energy of the surface chemical reaction has been estimated within a shrinking core particle and moving front model [37] from a set of isothermal TGA experiments using plots of $\ln[d\Delta W/dt]$ vs. $1/T$, where $d\Delta W/dt$ is the slope of the relative total weight change. The activation energies obtained vary between 28 and 142 kJ/mol [25].

The active phase of our catalysts for HDO occurs within the initial parabolic mass loss region, WO_3 to $WO_{2.9}$, for which activation energies have not been estimated. From mass conservation,

$$\frac{dm_O}{dt} = V(-rate) \quad (10)$$

where m_O is the mass of oxygen and V is the volume of the material. If we take the rate law to be first order in oxygen mass,

$$\frac{dm_O}{dt} = V\left(-k\frac{m_O}{V}\right) \quad (11)$$

Table 2
Composition of tungsten oxide bronzes, H_yWO_{3-z}, after hydrogen treatment as a function of temperature and further reduced WO_{3-x} after hydrogen removal as water.[a]

Catalyst (Surface Area)	Pan Material	Hydrogen Pretreatment Temperature/°C	y	z	Bronze H_yWO_{3-z}	x	Reduced WO_{3-x}
20 μm-WO_3 (1.5 m^2/g)	Ceramic	300	0.79	0.06	$H_{0.79}WO_{2.94}$	0.45	$WO_{2.55}$
		350	0.89	0.07	$H_{0.89}WO_{2.93}$	0.51	$WO_{2.49}$
		400	0.48	0.12	$H_{0.48}WO_{2.88}$	0.36	$WO_{2.64}$
		450	0.47	2.05	$H_{0.47}WO_{0.95}$	2.27	$WO_{0.73}$
UM-WO_3 (3.0 m^2/g)	Ceramic	200	0.93	0.06	$H_{0.93}WO_{2.94}$	0.52	$WO_{2.48}$
		300	1.11	0.08	$H_{1.11}WO_{2.92}$	0.63	$WO_{2.37}$
		350	1.29	0.23	$H_{1.29}WO_{2.77}$	0.88	$WO_{2.12}$
		400	0.77	1.13	$H_{0.77}WO_{1.87}$	1.51	$WO_{1.49}$
		450	0.21	2.84	$H_{0.21}WO_{0.16}$	2.95	$WO_{0.05}$
		475	0.29	2.80	$H_{0.29}WO_{0.20}$	2.95	$WO_{0.05}$
	Platinum	300	1.02	0.07	$H_{1.02}WO_{2.93}$	0.58	$WO_{2.42}$
		350	1.31	0.27	$H_{1.31}WO_{2.73}$	0.91	$WO_{2.09}$
		400	1.87	1.22	$H_{1.87}WO_{1.78}$	2.15	$WO_{0.85}$
		500	1.48	1.95	$H_{1.48}WO_{1.05}$	2.70	$WO_{0.30}$
nano-WO_3 (9.1 m^2/g)	Ceramic	300	1.22	0.12	$H_{1.22}WO_{2.88}$	0.73	$WO_{2.27}$
		325	0.95	0.22	$H_{0.95}WO_{2.78}$	0.70	$WO_{2.30}$
		350	1.28	0.25	$H_{1.28}WO_{2.75}$	0.95	$WO_{2.05}$
		400	0.80	2.40	$H_{0.80}WO_{0.60}$	2.80	$WO_{0.20}$
		450	0.25	2.59	$H_{0.25}WO_{0.41}$	2.72	$WO_{0.28}$
		475	0.09	2.89	$H_{0.09}WO_{0.11}$	2.93	$WO_{0.07}$

[a] At lower temperatures, the uncertainties are $y(\pm 0.05)$, $z(\pm 0.01)$, $x(\pm 0.02)$; at higher temperatures they are $y(\pm 0.3)$, $z(\pm 0.1)$, $x(\pm 0.05)$.

and recast the equation in terms of the total mass, m_t, tungsten mass, m_W, and initial oxide mass, m_i,

$$\frac{d(m_t/m_i)}{dt} = -k\left(\frac{m_t}{m_i} - \frac{m_W}{m_i}\right) \quad (12)$$

and use an Arrhenius expression for the rate constant, $k = A\exp(-E_a/RT)$ then taking the logarithm gives

$$\ln\left[\left.\frac{d(m_t/m_i)}{dt}\right|_z\right] = -\frac{E_a(z)}{RT} + \ln\left[A\left(\left.\left(\frac{m_t}{m_i}\right)\right|_z - \left(\frac{m_W}{m_i}\right)\right)\right] \quad (13)$$

where the rate of relative mass change is evaluated for a particular fractional mass loss, z, and the activation energy is allowed to be a function of the substoichiomety. This shows that a plot of the natural log of the slope vs. $1/T$, for the indicated fractional mass loss, should be linear with slope $-E_a/R$, and that the other factors all appear in the intercept.

Arrhenius plots are shown in Fig. 9 for each material at fractional masses of 99.99% ($WO_{2.998}$) and 99.5% ($WO_{2.93}$). The specific rate of reduction increases with surface area of the material, which is expected. At very small substoichiometry, the apparent activation energy, around 100 kJ/mol, is not significantly different for the three materials. However, the apparent activation energy decreased with increasing surface area at $m_t/m_i = 99.5\%$. For the low surface area 20 μm-WO_3, the apparent activation energy was 201 kJ/mol. The activation energy for the UM-WO_3 was 88 ± 7 kJ/mol and for the nano-WO_3 the apparent activation energy was 40 ± 13 kJ/mol. These values span the range of activation energies reported in similar experiments performed at much higher temperature conditions [25], suggesting that particle size effects may be important. In our experiments, the hydrogen content may be significantly higher than in the high temperature TGA measurements [25,37,38]; therefore, the reduction mechanism and activation energies may differ due to hydrogen content as well.

Clearly, the conditions required for catalyst pretreatment are sensitive to the WO_3 surface area, reduction time, and temperature. Both mass spectrometry data and theoretical calculations for oxygen defect creation mechanism are consistent with the reaction of hydrogen with lattice oxygen to form water and oxygen vacancies. In our work [23] and that of Tokarz-Sobieraj et al. [35], for MoO_3 surfaces, we argue that hydrogen dissociation must occur first to form surface hydroxyls, and then dehydroxylation leads to water desorption and surface oxygen vacancies. The initially large values of the effective activation energy at $m_t/m_i = 99.99\%$ may be due to a low population of surface hydroxyls, since the bulk sites are much more stable at low hydrogen content. A possible explanation for the decreased activation energies at $m_t/m_i = 99.5\%$ may be associated with the surface hydroxyl coverage. After an extended

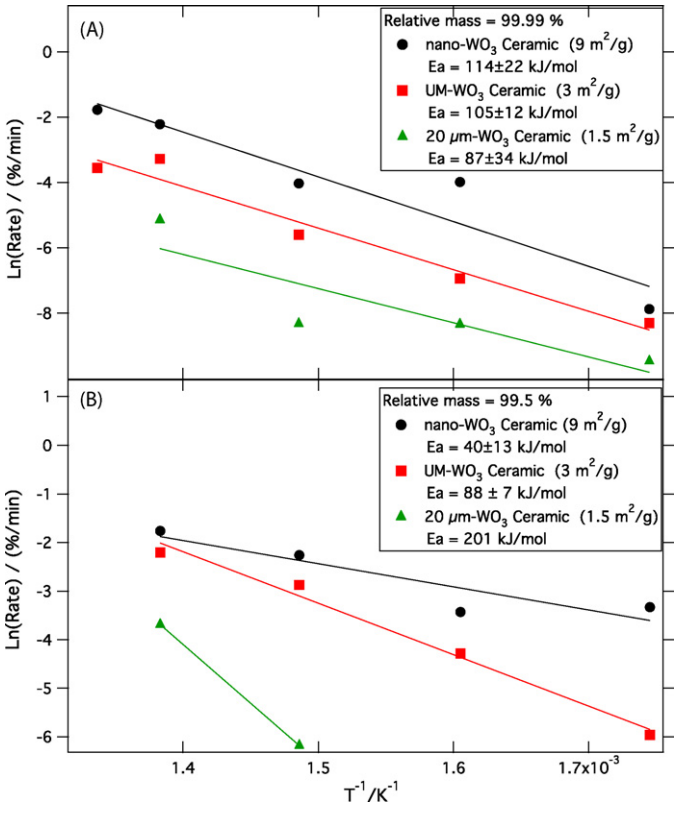

Fig. 9. Arrhenius plots for rate of reduction during hydrogen treatment of nano-WO_3, UM-WO_3, and 20 μm-WO_3 in ceramic TGA pans as indicated at a relative mass of (A) 99.99% ($WO_{2.998}$) and 99.5% ($WO_{2.93}$).

reduction period, during which hydrogen absorbs into the bulk, surface hydroxyl become energetically competitive with bulk sites and dehydroxylation become facile. The surface area dependence at $m_t/m_i = 99.5\%$ suggests that hydrogen content increases faster on higher surface area materials.

For the reaction of MoO_3 with H_2 to form water and surface oxygen vacancies, analogous to Reaction (1), we calculate $\Delta_r G = 74$ kJ/mol [23]. Oxygen vacancy diffusion is extremely fast [36] in MoO_3 and WO_3, and the oxide reduction rate is controlled by the surface reaction rates. From this perspective, the higher the specific surface area, the faster we would expect the rate of reduction of the oxide to be. Under flowing hydrogen conditions, we should not expect to achieve a true thermodynamic equilibrium, and so the steady state composition of the bronze need not be the same for the three materials, even if the physical state, and hence the $\Delta_r G$ for Reaction (1) were the same.

The differential heat of absorption of hydrogen into MoO_3 to form the bronze, H_aMoO_3, is large and negative at low hydrogen stoichiometry, a, decreases to zero around $a = 1$, and the reaction becomes endothermic for $a > 1$ [39]. At low composition, this reflects the electrostatic attraction between the protons dissolved in the bronze and lattice oxygen, implying a larger cohesive energy of the solid. To the extent that the hydrogen content of the bronzes varies among the three materials, we can expect the $\Delta_r G$ for Reaction (3) to be a function of hydrogen content, y. The apparent activation energies obtained (40–200 kJ/mol) for reduction of our reduced tungsten oxide bronze materials bracket the value calculated for dehydroxylation of surface hydroxyls from MoO_3 (74 kJ/mol) [23,35]. While differences in metal–oxygen bond strength certainly contribute to the magnitude of the reduction barrier, the presence of hydrogen in the bronze must also be a factor. Theoretical investigations of the effect of hydrogen in the bronze on dehydroxylation energies would be very helpful in distinguishing these effects.

4.3. Implications for catalyst pretreatment and reactivity

These results provide insight into several factors affecting the preparation and use of reduced tungsten oxide bronzes as a catalyst for hydrogenation (at 50 °C) and hydrodeoxygenation (at temperatures above 150 °C). When the catalyst is pretreated in hydrogen at temperatures close to the 300 °C threshold for loss of lattice oxygen, a steady state bronze composition can be achieved. The threshold temperature and treatment time appear to be sensitive to the specific surface area. To the extent that hydrogen may stabilize lattice oxygen, the hydrogen pretreatment pressure may also affect bronze composition.

The kinetics during reduction and bronze formation provide a guide to determining the catalyst pretreatment time. The reaction is exothermic and therefore accurate temperature control in the catalyst bed is required to reproducibly prepare the catalyst. We should also note that if the reduced catalyst (in the bronze state) was exposed to air, spontaneous combustion of the hydrogen and oxidation of the tungsten suboxide generates substantial heat, to the extent that it glowed orange. Thus, the catalyst needs to be maintained in an inert or reducing environment until reaction begins.

We found that only the UM-WO_3 was active for hydrogenation of acrolein to allyl alcohol, whereas all three tungsten oxide bronzes hydrogenated allyl alcohol to 1-propanol and catalyzed the isomerization to propanal. As already mentioned, this suggests that the sites for C=C hydrogenation are different from C=O hydrogenation. Our analysis of the adsorption energies for surface terminal, surface bridging, and bulk hydroxyl sites in the MoO_3 bronze system indicate that population of surface hydroxyls occurs only at fairly high hydrogen content (H_xMO_3, with $x \approx 1.1$–1.2). Thus it may be possible that for the UM-WO_3, with the highest hydrogen content, $H_{1.29}WO_{2.77}$, surface hydroxyl groups are populated and account for carbonyl hydrogenation. A possible explanation for C=C hydrogenation sites may be direct transfer of hydrogen from the bronze if allyl alcohol is adsorbed on oxygen vacancy sites. Further spectroscopic and theoretical work is needed to explore these potential reaction pathways.

These reactions occur at lower temperatures (50 °C) where the catalyst may or may not be able to adsorb hydrogen, but oxygen vacancy creation is negligible [27]. Therefore, if the catalyst is operated at temperatures below the threshold for rapid oxygen vacancy creation (which may be surface area and hydrogen partial pressure dependent), hydrogenation may be maintained at steady state, but hydrodeoxygenation cannot be sustained.

If the reaction temperature is increased above 150 °C hydrodeoxygenation activity is observed. At these temperatures production of propene and 1,5-hexadiene is observed and varies with time. We have proposed that the mechanism is closely related to the Mars–van Krevelen mechanism, as shown in Fig. 2. In one part of the catalytic cycle, hydrogen dissociates to form surface hydroxyls. The hydroxyls react with lattice oxygen to form water and create oxygen vacancies. Hydrogenation steps require protons, either from surface hydroxyls or directly from hydrogen atoms dissolved in the bronze. In the second part of the catalytic cycle, the alcohol adsorbs at a coordinatively unsaturated tungsten site (i.e. an oxygen vacancy), forming a relatively strong W–O bond and weakening the O–C bond. At this point, the propene radicals can desorb and couple to form 1,5-hexadiene [40–42] or they can pick up an additional hydrogen to form propene. It is important to note that the relative amounts of propene and 1,5-hexadiene vary with time online. In both processes the catalyst is left in a more oxidized state. Therefore, the H_yWO_{3-x} catalyst must be able to form oxygen vacancies again, as well as absorb hydrogen, in order to maintain a catalytic cycle at steady state.

From the time dependent product distribution, we can estimate the maximum amount of oxygen taken up by the catalyst in the hydrodeoxygenation reactions,

$$CH_2{=}CH{-}CH_2{-}OH\,(\text{allyl alcohol}) + V_O \rightarrow CH_2{=}CH{-}CH_3 + O_O \tag{14}$$

$$2CH_2{=}CH{-}CH_2{-}OH\,(\text{allyl alcohol}) + 2V_O \rightarrow CH_2{=}CH{-}CH_2{-}CH_2{-}CH{=}CH_2 + 2OH_O \tag{15}$$

where V_O represents a vacancy on an oxygen site. Notice that there is no net consumption or production of hydrogen in these reactions, but oxygen vacancies are annihilated. Loss of vacancies, as adsorption and reaction sites, would reduce the rate of these reactions if not regenerated. Oxygen vacancy creation occurs via the reactions

$$O_O + \tfrac{1}{2}H_2 \rightarrow OH_O \tag{16}$$

$$2OH_O \rightarrow H_2O(g) + O_O + V_O \tag{17}$$

In addition to the major HDO reaction products, we also observe production of propanal, acrolein and 1-propanol, from which we estimate the net consumption of hydrogen according to the reactions,

$$CH_2{=}CH{-}CH_2{-}OH\,(\text{allyl alcohol}) \rightarrow CH_3{-}CH_2{-}CH{=}O\,(\text{propanal}) \tag{18}$$

$$CH_2{=}CH{-}CH_2{-}OH\,(\text{allyl alcohol}) \rightarrow H_2{+}CH_2{=}CH{-}CH{=}O\,(\text{acrolein}) \tag{19}$$

$$H_2 + CH_2{=}CH{-}CH_2{-}OH\,(\text{allyl alcohol}) \rightarrow CH_3{-}CH_2{-}CH_2{-}OH\,(\text{1-propanol}) \tag{20}$$

Reaction (20) decreases and Reaction (19) increases the hydrogen content of the bronze while Reaction (18) does not change the bronze composition.

When the UM-WO_3 was reduced at 350 °C the composition of the bronze was determined to be $H_{1.29}WO_{2.77}$. After 5 h of reaction at 350 °C, 280 μmol of hydrogen was consumed by 1-propanol production and 330 μmol of oxygen was taken up by the catalyst. Assuming that no oxygen vacancy regeneration occurred, the final state of the catalyst would be $H_{1.23}WO_{2.85}$. This represents a maximum change in composition of the catalyst over 5 h of operation. Similarly, the nano-WO_3 would be converted from $H_{1.17}WO_{2.69}$ to $H_{0.84}WO_{2.74}$ and the 20 μm-WO_3 could be converted from $H_{0.89}WO_{2.94}$ to $H_{0.85}WO_{2.97}$. If we neglect catalyst regeneration during reaction it is evident that the state of the catalyst will approach WO_3 and become inactive for hydrodeoxygenation. As Fig. 8 shows, the HDO reaction rates decrease, as would be expected for a reversible $A \rightleftarrows B$ reaction approaching a steady state condition, in which the HDO Reactions (14) and (15) are competing with the oxygen vacancy Reactions (16) and (17). From thermogravimetric analysis we have estimated an oxygen vacancy creation barrier of order 140–200 kJ/mol. This is similar in magnitude to the barriers we have estimated for C–O bond scission on a Mo_3O_9 cluster of 104 kJ/mol [23]. Thus, we expect that at steady state, the bronze composition will approach an intermediate value between the initial composition of the bronze and the maximum values calculated above.

Similar arguments apply to the steady state hydrogen content of the catalyst in its active state. The observation that hydrogenation activity is relatively constant suggests that the dissociation of hydrogen on the bronze is sufficiently fast that the steady state hydrogen composition probably remains quite similar to the initial values.

Comparing the activity of the three materials for acrolein hydrogenation and allyl alcohol HDO reactions, the differences in surface area and crystallinity offer distinct opportunities to optimize a low temperature, first stage hydrotreatment reactor and a second stage, higher reaction temperature process, according to the general strategies previously employed [8]. The UM-WO_3 material was the only catalyst active for carbonyl hydrogenation, which appears to be related to the higher hydrogen content and more amorphous physical state. By contrast, the low surface area 20 μm-WO_3 showed the highest steady state selectivity toward HDO reactions. Once surface oxygen vacancies are created, maintaining a lower hydrogen content in the bronze may be preferable to suppress hydrogenation reactions.

5. Conclusions

From this study we have gained insight about the composition of tungsten oxide catalysts during pretreatment and under reaction conditions for the reduction of acrolein and allyl alcohol. Using thermogravimetric analysis under conditions of flowing hydrogen, nitrogen, and then oxygen, we have developed a method to determine the composition of tungsten oxide bronzes, H_yWO_{3-z}, from the relative weight changes. The evolved gases were monitored with a mass spectrometer. The net weight loss in the 300–500 °C hydrogen treatment step includes both weight loss due to removal of lattice oxygen and weight gain due to dissolution of hydrogen to form a bronze. Use of a platinum TGA pan increased the hydrogen composition, which appears to stabilize the lattice oxygen.

Using a catalyst pretreated at 350 °C, we have shown that tungsten oxide bronzes of form H_yWO_{3-z} are capable for the hydrogenation of allyl alcohol at lower temperatures (50–150 °C). More importantly, these same catalysts are capable of hydrodeoxygenation of this alcohol above 150 °C. We have shown that the active bronze (H_yWO_{3-z}) has the composition where $0.89 < y < 1.29$ and $0.07 < z < 0.31$.

Acknowledgements

We gratefully acknowledge support of this work through DOE Award #DE-FG02-07ER46373. The authors would like to thank Rachel Pollock and I. Tyrone Ghampson for the BET and XRD analysis of the tungsten oxide catalysts; Zhixiang Lu and Carl Tripp for synthesis of the UM-WO_3; and Rachel Austin for a critical reading of the manuscript.

References

[1] G.W. Huber, in: B. National Science Foundation. Chemical, Environmental, and Transport Systems Division (Ed.), NSF, Washington, DC, 2008.
[2] G.W. Huber, S. Iborra, A. Corma, Chemical Reviews (2006) 4044–4098.
[3] S.H. Beis, S. Mukkamala, N. Hill, J. Joseph, C. Baker, B. Jensen, E.A. Stemmler, M.C. Wheeler, B.G. Frederick, A. van Heiningen, A.G. Berg, W.J. DeSisto, BioResources 5 (2010) 1408–1424.
[4] L. Ingram, D. Mohan, M. Bricka, P. Steele, D. Strobel, D. Crocker, B. Mitchell, J. Mohammad, K. Cantrell, C.U. Pittman, Energy & Fuels 22 (2008) 614–625.
[5] C.A. Mullen, G.D. Strahan, A.A. Boateng, Energy & Fuels 23 (2009) 2707–2718.
[6] J. Joseph, C. Baker, S. Mukkamala, S.H. Beis, M.C. Wheeler, W.J. DeSisto, B.L. Jensen, B.G. Frederick, Energy & Fuels (2010), doi:10.1021/ef100504d.
[7] E. Furimsky, Catalysis Reviews, Science and Engineering 25 (1983) 421–458.
[8] D.C. Elliott, Energy & Fuels 21 (2007) 1792–1815.
[9] P. Claus, A. Bruckner, C. Mohr, H. Hofmeister, Journal of the American Chemical Society 122 (2000) 11430–11439.
[10] P. Claus, H. Hofmeister, C. Mohr, Gold Bulletin 37 (2004) 181–186.
[11] B. Coq, F. Figueras, P. Geneste, C. Moreau, P. Moreau, M. Warawdekar, Journal of Molecular Catalysis 78 (1993) 211–226.
[12] W. Grunert, A. Bruckner, H. Hofmeister, P. Claus, Journal of Physical Chemistry B 108 (2004) 5709–5717.
[13] C. Hoang-Van, O. Zegaoui, Applied Catalysis A: General 164 (1997) 91–103.
[14] T. Marinelli, S. Nabuurs, V. Ponec, Journal of Catalysis 151 (1995) 431–438.
[15] C. Mohr, H. Hofmeister, P. Claus, Journal of Catalysis 213 (2003) 86–94.
[16] C. Mohr, N. Hofmeister, M. Lucas, P. Claus, Chemical Engineering & Technology 23 (2000) 324–328.
[17] Y. Nagase, H. Hattori, K. Tanabe, Chemistry Letters (1983) 1615–1618.
[18] C. Hoang-Van, O. Zegaoui, Applied Catalysis A 130 (1995) 89–103.
[19] T. Matsuda, Y. Hirata, S. Suga, H. Sakagami, N. Takahashi, Applied Catalysis A 193 (2000) 185–193.
[20] J.E. Herrera, J.H. Kwak, J.Z. Hu, Y. Wang, C.H.F. Peden, J. Macht, E. Iglesia, Journal of Catalysis 239 (2006) 200–211.
[21] R.K. Grasselli, Topics in Catalysis 21 (2002) 79–88.
[22] P. Mars, D.W.V. Krevelen, Chemical Engineering Science 3 (Special Suppl.) (1954) 41.
[23] D.R. Moberg, T.J. Thibodeau, F.G. Amar, B.G. Frederick, Journal of Physical Chemistry C 114 (2010) 13782–13795.
[24] L. Bartha, A.B. Kiss, T. Szalay, International Journal of Refractory Metals & Hard Materials 13 (1995) 77–91.
[25] A. Lackner, T. Molinari, P. Paschen, Scandinavian Journal of Metals 25 (1996) 115–121.
[26] A.J.V. Hefedus, T. Millner, J. Neugebauer, K. Sasvári, Zeitschrift für Anorganische und Allgemeine Chemie 281 (1955) 64–82.
[27] K. Kanamaru, H. Kuwata, T. Okino, Thermochimica Acta 267 (1995) 117–127.
[28] K.M. Sancier, Journal of Catalysis 23 (1971) 298–300.
[29] P.A. Sermon, G.C. Bond, Catalysis Review 8 (1973) 211–239.
[30] Z. Lu, S.M. Kanan, C.P. Tripp, Journal of Material Chemistry 12 (2002) 983–989.
[31] E.P. Barrett, L.G. Joyner, P.P. Halenda, Journal of American Chemical Society 73 (1951) 373–380.
[32] M. Kruk, M. Jaroniec, A. Sayari, Langmuir 13 (1997) 6267–6273.
[33] S. Brunauer, P.H. Emmett, E. Teller, Journal of American Chemical Society 60 (1938) 309–319.
[34] M. Lu, MS Thesis, Chemistry, University of Maine, 2005.
[35] R. Tokarz-Sobieraj, M. Witko, R. Grybos, Catalysis Today 99 (2005) 241–253.
[36] E.R.S. Winter, Journal of Chemical Society (A). Inorganic Physics Theory (1968) 2889–2902.
[37] J.A. Bustnes, D. Sichen, S. Seetharaman, Metallurgical Transactions B 24B (1993) 475–480.
[38] R. Hasegawa, T. Kurosawa, T. Yagihashi, Transactions of JIM 15 (1974) 75–82.
[39] X. Sha, L. Chen, A.C. Cooper, G.P. Pez, H. Cheng, Journal of Physical Chemistry C 113 (2009) 11399–11407.
[40] B. Grzybowska, J. Haber, J. Janas, Journal of Catalysis 49 (1977) 150–163.
[41] W. Martir, J.H. Lunsford, Journal of American Chemical Society 103 (1981) 3728–3732.
[42] P.J. Hart, H.R. Friedli, Journal of Chemical Society (D) (1970) 621–622.